Marine Geology 465 (2023) 107164

Contents lists available at ScienceDirect

Marine Geology

journal homepage: www.elsevier.com/locate/margo

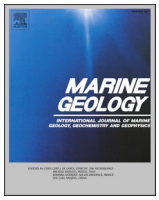

Revisiting the South China Sea MORBs: Mg isotope and whole-rock geochemical constraints

Yidi Hong [a,b], Tao Wu [a,b,c,*], Chunfeng Li [a,b], Xuegang Chen [a,b], Jianggu Lu [c], Haiou Gu [d], Rong Xu [e]

[a] Hainan Institute of Zhejiang University, Sanya 572025, China
[b] Ocean College, Zhejiang University, Zhoushan 316021, China
[c] Key Laboratory of Submarine Geosciences, Ministry of Natural Resources, Hangzhou 310012, China
[d] School of Resources and Environmental Engineering, Hefei University of Technology, Hefei 230009, China
[e] State Key Laboratory of Ore Deposit Geochemistry, Institute of Geochemistry, Chinese Academy of Sciences, Guiyang 550081, China

ARTICLE INFO

Editor: Dr. Adina Paytan

Keywords:
South China Sea
Magnesium isotope
Mid-Ocean Ridge Basalts
Olivine accumulation
Hainan Mantle Plume

ABSTRACT

Mid-Ocean Ridge Basalts (MORBs) from the South China Sea (SCS) have attracted great attention from geologists in the past decade, but their petrogenesis still remains controversial. Here, we show that the Mg isotopes of MORBs from Integrated Ocean Drilling Program (IODP) Sites U1431, U1433 and U1434 are heterogeneous and present the mechanisms causing such heterogeneity. The MORBs from Sites U1431, U1433 and U1434 have δ^{26}Mg values ranging from −0.35‰ to −0.21‰, from −0.34‰ to −0.13‰, and from −0.30‰ to −0.20‰, respectively. Together with all the published data, we found the MORBs at Site U1431 with high MgO contents (> 9 wt%) usually have δ^{26}Mg values that are generally lower than the normal mantle (−0.25‰ ± 0.04‰), whereas some of the Site U1433 MORBs are higher than the normal mantle. Shallow-level geological processes like seawater alteration have negligible effects on the Mg isotope fractionation of our samples. Elemental ratio indicative of the degree of partial melting (like Sm/Nd) from the same site also shows no relationship with the δ^{26}Mg variations. Olivine is proposed to have light Mg isotopes. Considering the high MgO (> 9 wt%) contents of low-δ^{26}Mg samples and the petrographic evidence, we propose that their slightly light Mg isotopic compositions of U1431 MORBs may result from the enrichment of olivine, rather than reflecting the mantle source. Moreover, low Ce/Pb ratios and most variable δ^{26}Mg values of some U1433 MORBs suggest that lower continental crustal materials have contributed to their source. As all the previously published MORBs are evolved, we use the *Revpet* to estimate the mantle melting conditions of SCS MORBs, including the Site U1500 samples recovered from the northern margin of SCS. Compared with the global MORBs data, there is no thermal anomaly in SCS MORBs. Together with our new Mg isotope data, therefore, we propose that the role of the Hainan mantle plume in the opening and spreading of the SCS may be insignificant.

1. Introduction

It is well known that the geochemical and isotopic compositions of the Earth's mantle are heterogeneous (Hofmann, 1997; le Roux et al., 2002; Niu et al., 1996). Oceanic basalts, which are produced by partial melting of the mantle, carry abundant messages from their source. They are of great significance for investigating mantle composition, tectonic and dynamic mechanism of the Earth's interior, and are considered as important objects for studying the large-scale heterogeneity of the mantle (Sun and McDonough, 1989).

As a common type of oceanic basalts, mid-ocean ridge basalts (MORBs), produced by high degree of partial melting of the mantle, are the most abundant igneous rocks on the Earth's surface (Niu, 2016). MORBs can be divided into two main types based on their trace elemental and isotopic differences, i.e., incompatible-element-depleted normal (N-MORB) and incompatible-element-enriched (*E*-MORB) basalts. Such compositional differences in MORBs can reflect the crust and mantle thermal structure, magma temperature, and the degree of magma differentiation and homogenization (Rubin and Sinton, 2007). The geochemical characteristics of MORB samples, including their major

* Corresponding author at: Hainan Institute of Zhejiang University, Sanya 572025, China.
E-mail address: taowu@zju.edu.cn (T. Wu).

https://doi.org/10.1016/j.margeo.2023.107164
Received 7 June 2023; Received in revised form 5 October 2023; Accepted 7 October 2023
Available online 10 October 2023

and trace elemental abundances and ratios, stable and radiogenic isotopes, can also help to elucidate the evolution histories of their mantle sources (Langmuir and Hanson, 1980; Natland, 1989).

Magnesium (Mg) is a major constituent of the silicate Earth, hydrosphere and biosphere (McDonough and Sun, 1995; Millero, 1974; Teng et al., 2010). The cycle of Mg experiences the initial extraction from the mantle, storage in igneous rocks in the crust, transportation to the hydrosphere due to weathering, and return to the mantle by subduction (Guo et al., 2019). Mg isotope is one of the non-traditional stable isotopes concerned with the geochemical processes. There are three stable isotopes of Mg, ^{24}Mg, ^{25}Mg, and ^{26}Mg, with typical abundances of 78.99%, 10.00% and 11.01%, respectively (Berglund and Wieser, 2011). The relative mass difference between ^{24}Mg and ^{26}Mg reaches to 8%, contributing to significant mass fractionation of Mg during many geological processes. During low-temperature processes, Mg isotopes are fractionated largest and during high-temperature processes, they are less fractionated (Teng et al., 2010; Teng, 2017). Hence, the Mg isotopic composition can be a potential geochemical tracer, which is commonly applied to constrain the mantle source compositions of oceanic basalts (Teng, 2017).

The South China Sea (SCS) has undergone a long period of tectonic and magmatic evolution. Based on the Quaternary igneous rocks in the SCS and its surrounding areas, previous studies have demonstrated that the upper mantle of SCS is highly heterogeneous (Li et al., 2013; Qian et al., 2020; Zhang et al., 2020). Not only the radiogenic Sr-Nd-Hf-Pb isotopes, but also the stable metal Fe—Mg isotopes exhibit a large variation. The International Ocean Discovery Program (IODP) Expedition 349 drilled into the basement of SCS and recovered MORBs samples from Site U1431 in the Eastern subbasin, and Sites U1433 and U1434 in the Southwest subbasin (Fig. 1, Li et al., 2014a), providing an excellent opportunity to investigate the nature of the sub-ridge mantle. A hypothesis of the mantle plume has been raised to explain the geochemical and petrologic natures of the SCS (Flower et al., 1998; Xu et al., 2012; Zhang et al., 2018a, 2018b). It was proposed that a thermal anomaly existed in Site U1431 (Yang et al., 2019), which may result from the Hainan mantle plume. Carbonates are enriched in lighter Mg isotopes than the mantle (Higgins and Schrag, 2010; Teng et al., 2010), and therefore, recycled carbonates in the mantle source can lead to extremely light Mg isotopes of basalts (Li et al., 2021). The typical Hainan plume-derived Cenozoic basalts are reported to have lower δ^{26}Mg values than the normal mantle, which may be caused by sedimentary carbonates recycled into the upper mantle during subduction (Li et al., 2017). However, previous studies have shown that the U1431 basalts exhibit mantle-like Mg isotopic compositions (Liao et al., 2022a; Zhong et al., 2021) and suggested that such normal values may be generated by mixing of two-endmember mantle source, in which the Hainan mantle plume may contribute to a light-δ^{26}Mg endmember (Zhong et al., 2021). However, the role of the Hainan mantle plume in the generation of the SCS MORBs is still not fully understood. Furthermore, the heavier δ^{26}Mg signatures of U1433 basalts have been reported, which are accounted for the contribution of either recycled subarc lithosphere (Zhong et al., 2021) or high-δ^{26}Mg fluids released during subduction (Liao et al., 2022a). However, as the mantle source of U1433 basalts was considered to have been contaminated by lower continental crust (LCC) (Wu et al., 2023; Zhang et al., 2018a), whether the LCC can exert an influence on the Mg isotopic compositions of U1433 basalts is still unclear.

In this study, we present eighteen new Mg isotopic data of MORBs from Sites U1431, U1433 and U1434, SCS. Together with all the published major, trace element and Mg isotopic data of MORBs from the

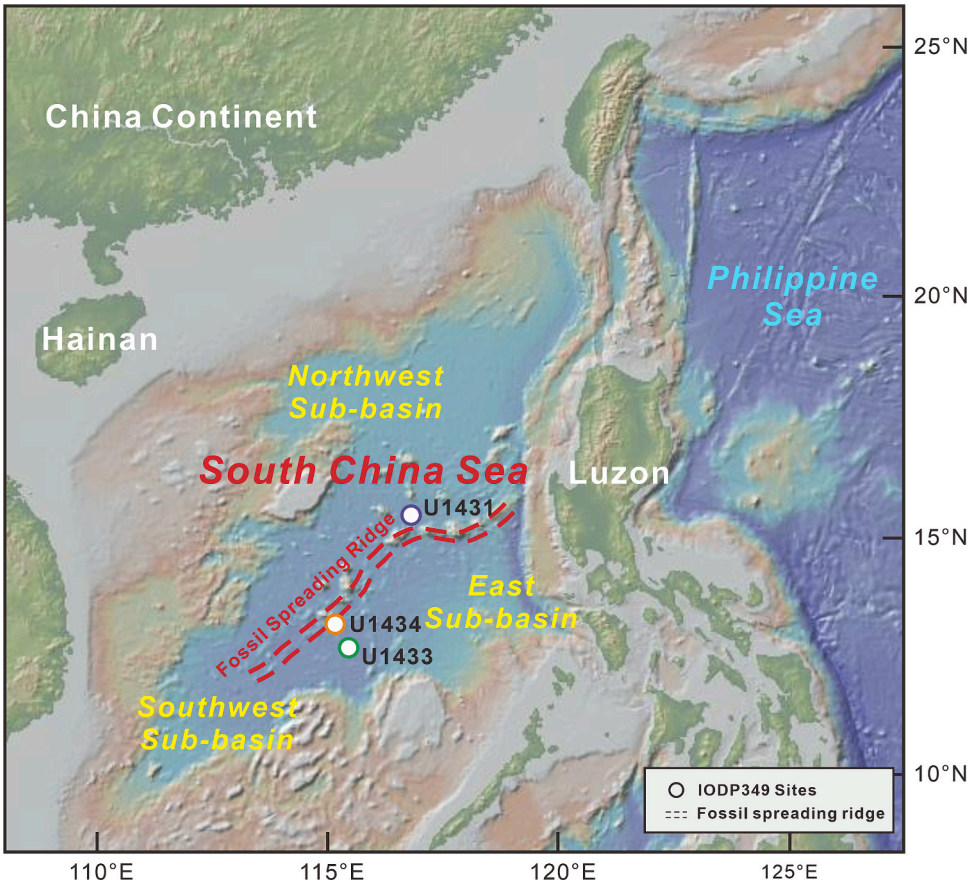

Fig. 1. Topographic map showing the South China Sea (SCS) and surrounding area. Locations of drilling sites (U1431, U1433 and U1434) are marked with circles in different colors, they are all from IODP Expedition 349. The base map was downloaded from http://www.geomapapp.org/.

SCS, we aim to (1) decipher the behaviors of Mg isotopes during magmatism and their implications for magmatic evolution; and (2) re-evaluate the role of lower continental crust and the Hainan mantle plume in the generation of the SCS MORBs.

2. Geological setting and sampling

The SCS is located at the junction of the Eurasian, Indo-Australian, and Philippine plates. IODP Expedition 349 conducted in 2014 first reported that the opening age of the SCS is ~33 Ma through high-resolution deep-tow magnetic anomalies (Li et al., 2014b). And for the first time, the IODP Expedition 349 scientists cored into the oceanic basement of the SCS and obtained basalt samples from three Sites (U1431, U1433 and U1434, Fig. 1).

Although the evolution history is relatively short, the SCS has experienced continental rifting during the latest Cretaceous to Paleogene, and subsequent seafloor spreading in the Oligocene to middle Miocene, then to subduction in early Middle Miocene (Cullen et al., 2010; Franke et al., 2014), along with extensive intraplate volcanism (Yan et al., 2006). With the above basic elements, the SCS is supposed to have undergone a nearly complete Wilson Cycle (Ding et al., 2018), making it an ideal area for studying complicated tectonic and magmatic activities.

The deep-water basin of the SCS can be divided into three subbasins, the East, the Northwest, and the Southwest subbasins (Fig. 1). Among these three subbasins, the East subbasin is the largest and was formed by North-South extension (Zhang et al., 2018a). The Southwest subbasin is a V-shaped propagating rift and has a deeper average water depth than the East subbasin (Ding et al., 2016). The MORBs of the East and the Southwest subbasins show great geochemical variation in the temporal and spatial distribution. Their Sr-Nd-Hf-Pb isotopic compositions exhibit Indian-type MORBs. Based on the trace element compositions, the East subbasin is composed of both N- and E-MORBs with a radiogenic isotopically depleted MORB mantle (DMM) source, whereas those in the Southwest subbasin are mainly E-MORBs (Zhang et al., 2018a).

A total of 18 basalt samples from the IODP Expedition 349 (6 samples from Site U1431, 7 samples from U1433 and 5 samples from U1434) are selected for our study (Figs. 1 and 2). The Site U1431 was drilled 118.01 m beneath the top of the igneous basement in the East subbasin, two basalt layers at 890.0–962.5 and 972.0–1007.9 mbsf (meters below seafloor) were recovered there (Li et al., 2014b). Sites U1433 and U1434 were both located at the Southwest subbasin, and U1434 was closer to the fossil spreading ridge (Fig. 1). Basalts at Site U1433 were identified between 786.3 and 858.5 mbsf, and basalts at Site U1434 were recovered at 278.3–308.7 mbsf (Zhang et al., 2018a). According to our previous studies (Sun, 2020; Sun et al., 2020), the basalt samples from Site U1431 are N-MORB-like, and the basalt samples from Site U1433 and U1434 are E-MORB type.

Under the microscope (Fig. 3a, b and c), the samples from Site U1431 present a porphyritic texture with olivine and plagioclase phenocrysts in a groundmass of plagioclase and clinopyroxene. Most of the olivine phenocrysts have grain sizes of 0.1–0.5 mm, from euhedral to subhedral, whereas some of them are anhedral and > 1 mm in size. Specifically, large amounts of olivine phenocrysts were observed in U1431 samples, which have high MgO contents (e.g., 349-U1431E-37R-1-W, 58/60 in Fig. 3a and 349-U1431E-40R-2-W,45.5/48 in Fig. 3b). Samples from Site U1433 have plagioclase and olivine phenocrysts with assemblages of clinopyroxene and plagioclase in their groundmass (Fig. 3d, e and f). The grain sizes are relatively smaller than that of U1431. Site U1434 samples mainly consist of acicular plagioclase, glassy and cryptocrystalline groundmass. Some of them have olivine as the only phenocryst (Fig. 3g, h and i).

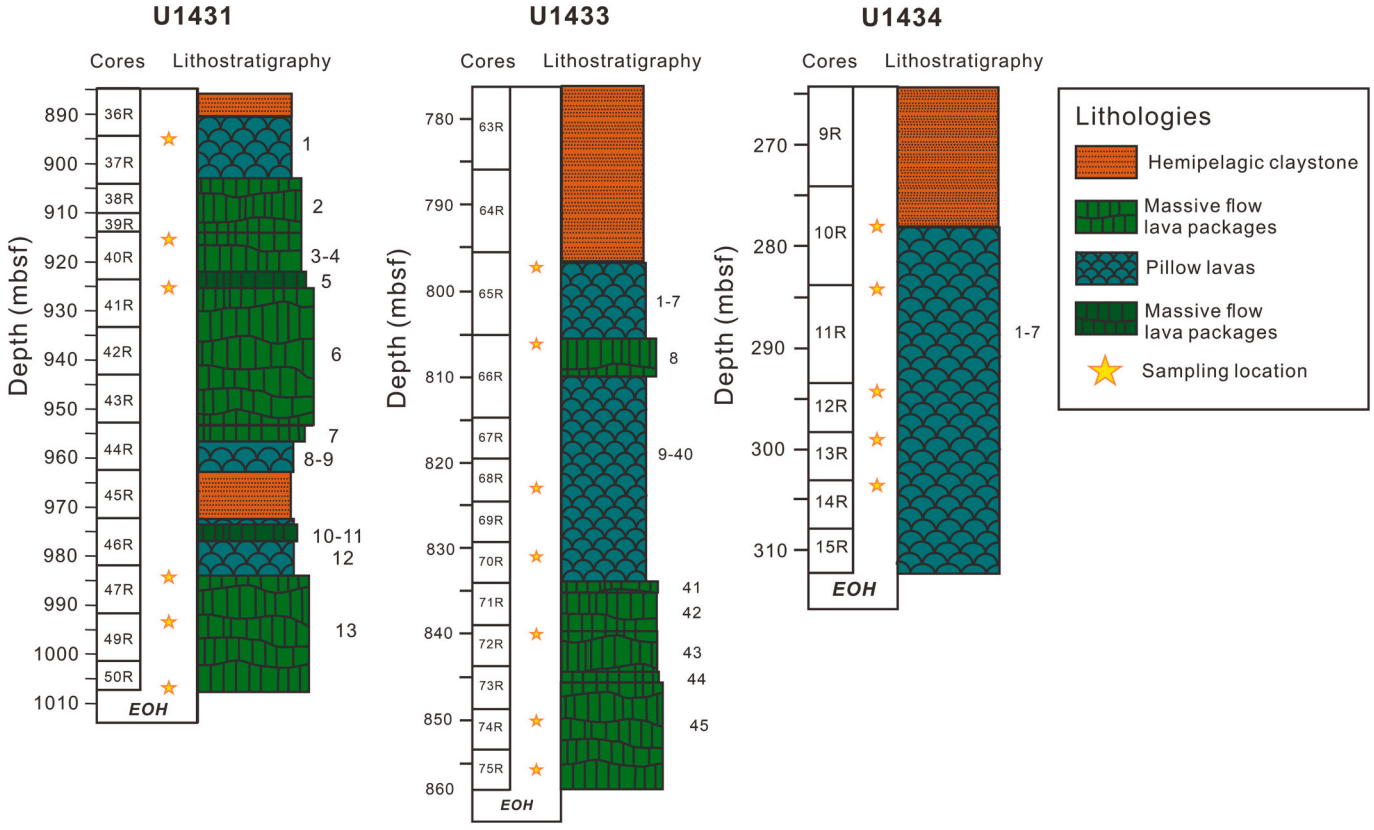

Fig. 2. Lithologies of three drilling sites and the exact sampling locations (modified from Li et al. (2014b)). The yellow five-pointed stars represent samples determined for Mg isotopes in this study. (For interpretation of the references to colour in this figure legend, the reader is referred to the web version of this article.)

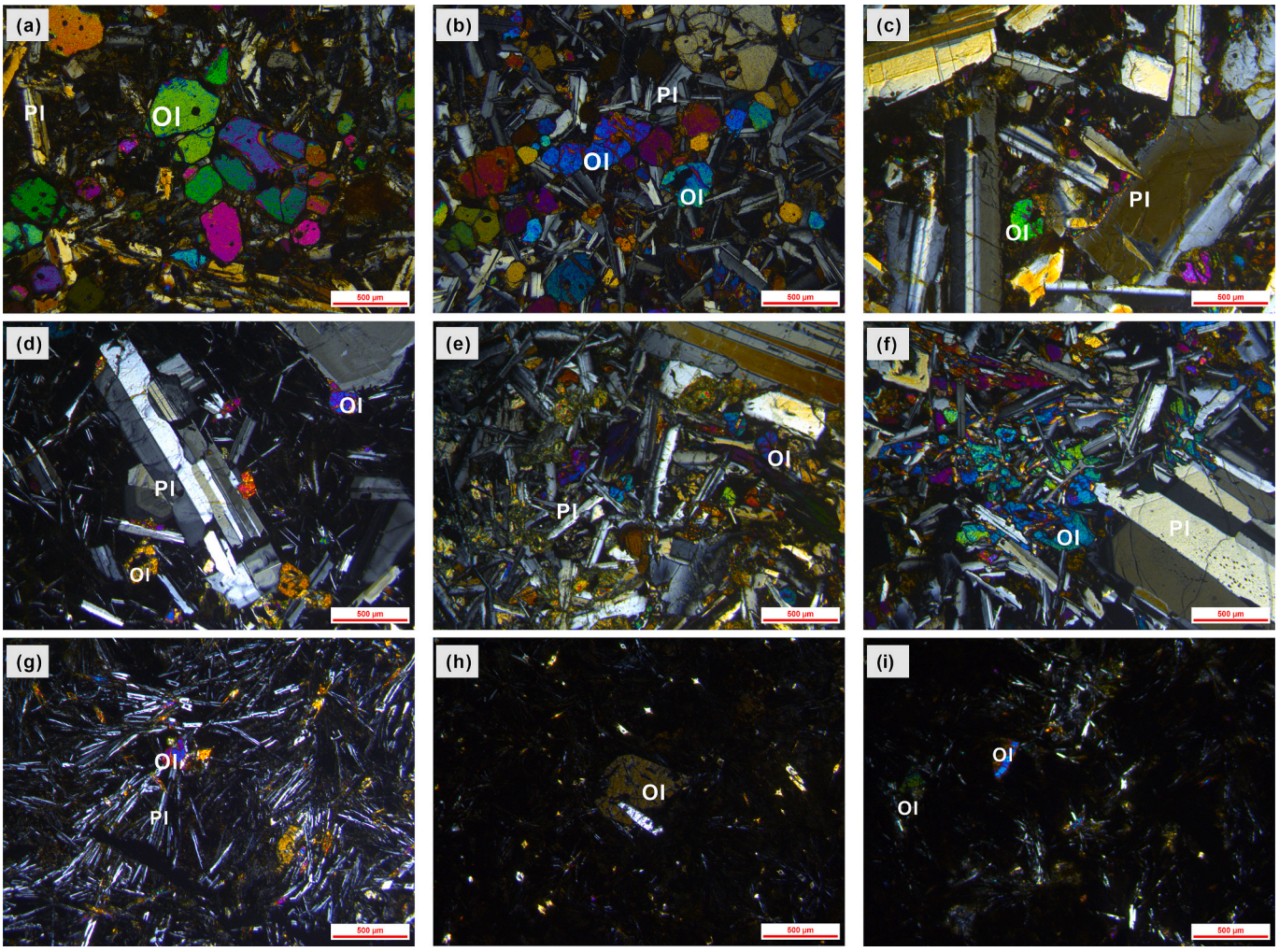

Fig. 3. Microscopic images of the Cenozoic basalt samples from Site U1431, U1433 and U1434. (a) 349-U1431E-37R-1-W, 58/60; (b) 349-U1431E-40R-2-W,45.5/48; (c) 349-U1431E-50R-5-W, 45.5/47.5; Plagioclase and olivine phenocrysts can be seen in the U1431 samples; (d) 349-U1433B-65R-2-W,96.0/98.0; (e) 349-U1433B-66R-1-W,117/119.6; (f) 349-U1433B-74R-1-W,66.5/68.5; The grain sizes of olivine phenocrysts of U1433 samples are smaller than the U1431; (g) 349-U1434A-11R-1-W,93.5/95.5; (h) 349-U1434A-14R-1-W,47/49; (i) 349-U1434A-13R-1-W,58.5/64.5; The U1434 samples have olivine as the only phenocryst. Abbreviations: Ol- olivine; Pl- plagioclase.

3. Analytical methods

The Mg isotopic analysis was performed by using a ThermoFisher Neptune Plus Multi-Collector Inductively Coupled Plasma Mass Spectrometer (MC-ICP-MS) at the Ore Deposit and Exploration Centre, Hefei University of Technology. The following procedures were carried out using the description of Huang et al. (2021). Every 10–20 mg sample powder was dissolved in a 2:1 mixture of concentrated HF: HNO_3, and then heated continuously and evaporated until dry. After adding a concentrated aqua regia (HCl: HNO_3 = 3:1), the mixture was reheated to dryness. 0.5 N HNO_3 was finally added when the solution became completely dried.

The separation of Mg isotopes in solution was completed with an AG50W-X8 resin (200–400 meshes, about 2.7 ml). The analytical quality was monitored by the international rock standards (BCR-2 and BHVO-2), blank samples and replicate samples. The results were reported in the form of δ-DSM3:

$$\delta^{X}Mg = \left[\left({}^{X}Mg/{}^{24}Mg \right)_{sample} - \left({}^{X}Mg/{}^{24}Mg \right)_{DSM3} - 1 \right] \times 1000 \quad (1)$$

where X = 25 or 26. The long-term external reproducibility (2SD) was better than 0.06‰ for δ^{26}Mg based on repeated analysis of synthetic solutions and rock standards (Huang et al., 2021).

4. Results

Analytical results of those 18 basalt samples are presented in Table 1 and shown graphically in Fig. 4. Two rock standards (BHVO-2 and BCR-2) yield δ^{26}Mg values of −0.24 ± 0.04‰ (2SD, n = 2) and − 0.19 ± 0.01‰ (2SD, n = 2), respectively, which agree with the reference values within the error (An et al., 2014; Huang et al., 2021). The δ^{26}Mg values of basalts at Site U1431 vary from −0.35 ± 0.06‰ to −0.21 ± 0.01‰ with an average of −0.29 ± 0.04‰ (2SD, n = 6), are similar or slightly lower than the normal mantle (−0.25 ± 0.04‰, Teng et al., 2010). Additionally, the δ^{26}Mg values of basalts at Site U1433 varies from −0.34 ± 0.08‰ to −0.13 ± 0.02‰ with an average of −0.24 ± 0.03‰ (2SD, n = 7), and the Site U1434 basalts have δ^{26}Mg values ranging from −0.30 ± 0.02‰ to −0.20 ± 0.07‰ with an average of −0.27 ± 0.05‰ (2SD, n = 5). Site U1434 has average δ^{26}Mg values that are similar to the normal mantle, whereas some of the U1433 samples present distinct higher δ^{26}Mg values (Fig. 4). The major and trace element compositions of those basalts are from Sun (2020). In general, they are classified as sub-alkaline series based on the TAS diagram, and show tholeiitic characteristics on the diagram of K_2O-SiO_2. Site U1431 basalts show trace element patterns similar to the N-MORB, whereas U1433 and U1434 basalts show E-MORB-like trace element patterns.

Table 1
Magnesium isotopic compositions of the Cenozoic basalts from the SCS.

Sample	δ^{25}Mg (‰)	2SD	δ^{26}Mg (‰)	2SD	N
349-U1431E-37R-1-W,58/60	−0.17	0.06	−0.35	0.06	2
349-U1431E-40R-2-W,45.5/48	−0.16	0.03	−0.31	0.01	2
349-U1431E-41R-2-W,133/136	−0.12	0.03	−0.31	0.03	2
349-U1431E-47R-3-W,60/62	−0.13	0.01	−0.27	0.03	2
349-U1431E-49R-2-W,66.5/68.5	−0.18	0.05	−0.28	0.10	2
349-U1431E-50R-5-W,45.5/47.5	−0.10	0.01	−0.21	0.01	2
349-U1433B-65R-2-W,96.0/98.0	−0.17	0.01	−0.28	0.03	2
349-U1433B-66R-1-W,117/119.6	−0.16	0.03	−0.33	0.07	2
349-U1433B-68R-3-W,74/76	−0.06	0.05	−0.19	0.01	2
349-U1433B-70R-2-W,29/32	−0.06	0.01	−0.13	0.02	2
349-U1433B-72R-1-W,81/84	−0.12	0.02	−0.24	0.01	2
349-U1433B-74R-1-W,66.5/68.5	−0.16	0.05	−0.34	0.08	2
349-U1433B-75R-3-W,28.5/30.5	−0.08	0.01	−0.16	0.01	2
349-U1434A-10R-CC-W,20/22	−0.15	0.14	−0.28	0.05	2
349-U1434A-11R-1-W,93.5/95.5	−0.11	0.05	−0.30	0.02	2
349-U1434A-12R-1-W,10/15	−0.12	0.01	−0.20	0.07	2
349-U1434A-13R-1-W,58.5/64.5	−0.13	0.04	−0.28	0.07	2
349-U1434A-14R-1-W,47/49	−0.14	0.08	−0.28	0.02	2
349-U1434A-14R-1-W,47/49-repeat	*−0.15*	*0.05*	*−0.26*	*0.03*	*2*
Standards					
BHVO-2	−0.09	0.02	−0.24	0.04	2
BCR-2	−0.10	0.02	−0.19	0.01	2

$\delta^{X}Mg = [(^{X}Mg/^{24}Mg)_{sample} - (^{X}Mg/^{24}Mg)_{DSM3} - 1] \times 1000$, where X = 25 or 26.

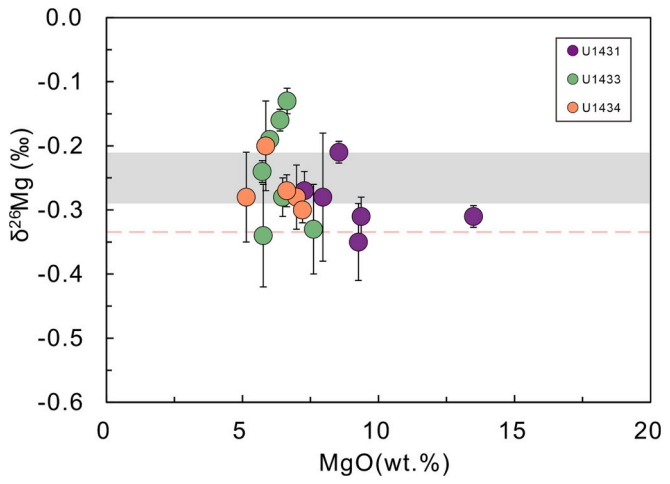

Fig. 4. Variations in δ^{26}Mg values versus MgO contents for the basalts from the SCS. The horizontal grey bar stands for the δ^{26}Mg values of the normal mantle (−0.25 ± 0.04‰, 2SD, Teng et al., 2010), and the pink dotted line is the average δ^{26}Mg values of Hawaii basalt olivine (−0.336 ± 0.026‰, 2SE, Young et al., 2009). The vertical black lines represent 2SD uncertainties. (For interpretation of the references to colour in this figure legend, the reader is referred to the web version of this article.)

5. Discussion

5.1. Effects of shallow-level geological processes

Seawater alteration is a major shallow geological process that may lead to the Mg isotopic variation of the oceanic basalts. Seawater can be considered homogeneous with a δ^{26}Mg value of −0.82 ± 0.01‰ (Foster et al., 2010). When the seawater interacts with the basalts, δ^{26}Mg values and most trace element concentrations and ratios are considerably modified (Verma, 1992).

Seawater alteration can exert influences on the element fluxes in the ocean, especially on fluid-mobile elements like Th and Cs (Verma, 1981, 1992). Meanwhile, the lithophile refractory element like Nb is fluid-immobile (Jochum and Verma, 1996) and acts as a highly incompatible element in all oceanic basalts (Hofmann et al., 1986). These elements are suitable indicators for seawater alteration. Besides, Cs is mobile while Ti is relatively fluid-immobile during seafloor alteration, Cs/TiO_2 can be used to assess the alteration-induced changes (Zhang and Smith-Duque, 2014). In this study, the fluid-mobile elements (e.g., Th) and fluid-immobile elements (e.g., Nb and Zr) present favorable positive correlations (Fig. 5), suggesting that the alteration, which may interfere with the correlations, is insignificant. This is also confirmed by the observation of thin sections under the microscope, which has shown that all the studied basalts are fresh (Fig. 3). Furthermore, the δ^{26}Mg values of SCS MORBs do not show any correlation with the loss-on-ignition (LOI) or Cs/TiO_2 values (Fig. 5). The possibility of seawater alteration causing the Mg isotopic variation can thus be ruled out.

As the indicator of basaltic crystallization differentiation, the $Mg^{\#}$ values (molar 100 * MgO / (MgO + TFeO)) of SCS basalts range from 32.8 to 75.2, with most of them being lower than the value of primary magma ($Mg^{\#} > 70$). Some of the U1431 basalts with high $Mg^{\#}$ values were observed to contain large amounts of olivine (e.g., U1431E-43R-2 W 6/10 and U1431E-42R-1 W 25/30 from Liao (2020)). Together with all the published data, the basalts show broad scatter in SiO_2, TiO_2, Al_2O_3, and TFeO versus $Mg^{\#}$ diagrams (Fig. S1). The Ni and Cr contents show positive correlations with $Mg^{\#}$, indicating that those basalts have undergone mineral fractional crystallization.

We used the *ReversePetrogen* (*Revpet*: a computing method for evolved basalts, Krein et al., 2021) to investigate the fractional crystallization conditions and to determine which minerals were involved in the fractional crystallization. *Revpet* provides an algorithm for dry, tholeiitic and alkaline basalts, and acts as a multiphase dry reverse fractional crystallization and mantle melting thermobarometer (Krein et al., 2021). Based on the saturation sequence of mineral phases during tholeiitic differentiation, that is, olivine (O) is the first mineral that crystallized and fractionated, then the olivine and plagioclase (OP), finally the olivine, plagioclase and augite/clinopyroxene (OPA). Meanwhile, the primary melts will evolve from a higher $Mg^{\#}$ value that equilibrated with the mantle to a comparatively lower $Mg^{\#}$ value. *Revpet* therefore uses variables $Mg^{\#}_{OP}$ and $Mg^{\#}_{OPA}$ to measure the above transition process and deduce the melt composition. The $Mg^{\#}$ value of primary mantle melts, $Mg^{\#}_{pri}$ acts as the ending point of the calculation. The reversed fractionation crystallization paths and corresponding erupted basalt can thus be simulated by setting $Mg^{\#}_{OP}$, $Mg^{\#}_{OPA}$ and $Mg^{\#}_{pri}$ values. The simulated results in Fig. 6 showed that the primary magma of SCS basalts may have undergone the fractional crystallization of olivine, clinopyroxene and plagioclase, some of the basalts in Site U1431 have only undergone the olivine fractional crystallization. However, no obvious fractional crystallization path of plagioclase can be found in Fig. 6, suggesting the crystallization of plagioclase may be insignificant, which is also confirmed by the no negative Eu anomaly in the incompatible trace element distribution pattern of the SCS basalts (Fig. S2). Previous study has illustrated that no detectable Mg isotopic fractionation can be caused by fractional crystallization of olivine and pyroxene (Teng et al., 2007). There is also no correlation between δ^{26}Mg values and MgO, TFeO and CaO/Al_2O_3 (Fig. S3). Therefore, the mineral fractional crystallization may have insignificant effect on Mg isotopes.

5.2. The Mg isotope heterogeneity in SCS MORBs: Causes and implications

Since the seawater alteration and mineral fractional crystallization have limited effect, the Mg isotopic heterogeneity of SCS basalts may be inherited from the source composition. Previous study on the Cenozoic basalts from the South China Block suggests that the degree of partial melting can also affect their δ^{26}Mg isotopes (Huang et al., 2015). If two elements have similar compatibility during partial melting, their elemental ratios in the melt are largely controlled by the source composition. Otherwise, the degree of partial melting can dominate

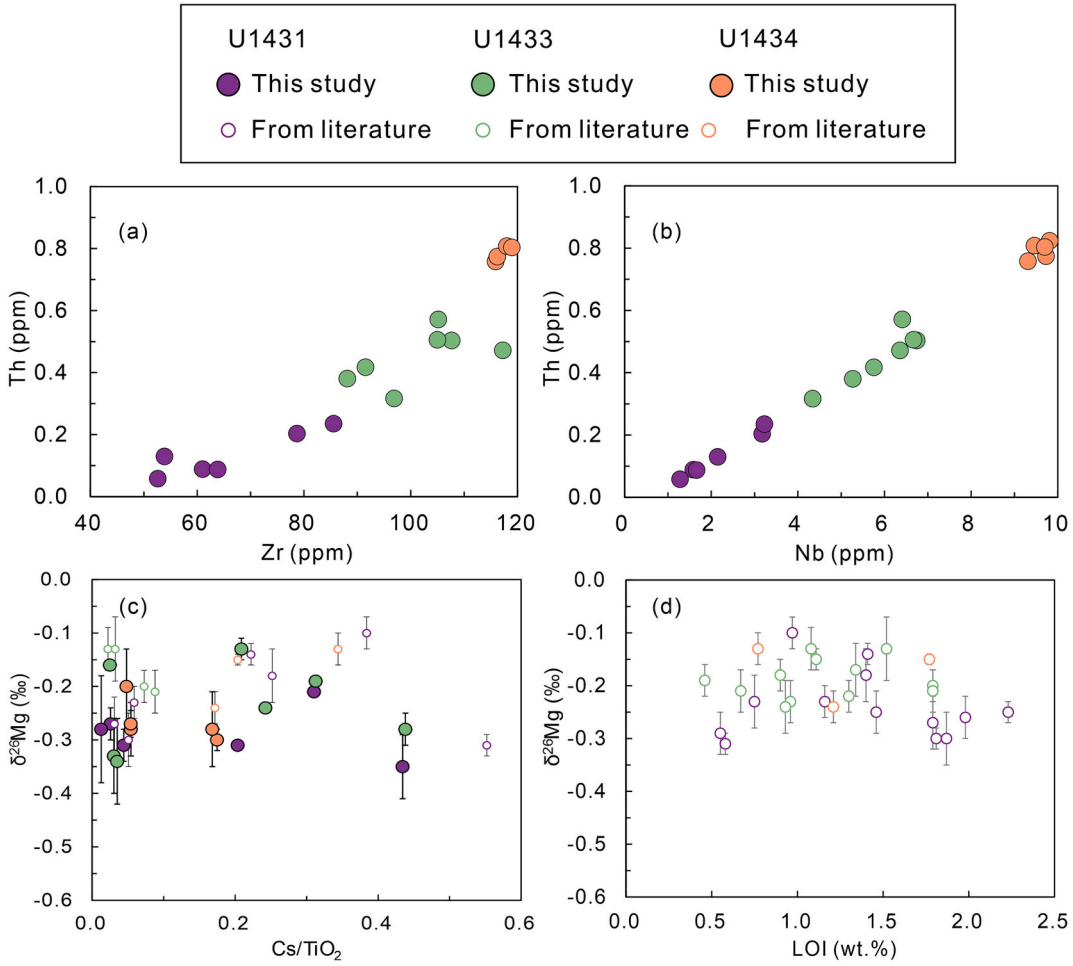

Fig. 5. (a) and (b) are fluid-mobile element Th versus fluid-immobile elements Zr and Nb. The good correlations suggest that the studied SCS samples were not affected by seawater alteration; (c) and (d) are Cs/TiO_2 and LOI versus $\delta^{26}Mg$ values of the SCS basalts, no correlation between them indicates seawater alteration has limited effect on Mg isotopes of the SCS basalts. Circles in larger sizes represent data in this study. Hollow circles in smaller sizes are data from other literature (Liao et al., 2022a; Zhong et al., 2021).

their composition in the melt if two elements have obviously different compatibility. Therefore, plots of such elemental ratios vs. $\delta^{26}Mg$ values can be used to investigate the role of partial melting in Mg isotopic variations of our samples (Zhong et al., 2017). The correlations between $\delta^{26}Mg$ values and selected trace elemental ratios of our samples are shown in Fig. 7. Incompatible elements in Fig. S2 show that the U1431 has the highest degree of partial melting and the U1434 has the lowest. However, in each site, the elemental ratio concerning the degree of partial melting (like Sm/Nd) shows no appreciable correlation with Mg isotopic compositions of the samples (Fig. 7a). The model of Mg isotopic fractionation in the partial melting of spinel peridotite illustrates that the $\delta^{26}Mg$ values of melts have positive correlations with the degree of melting, low-degree of melting can contribute to slightly lower $\delta^{26}Mg$ values (Zhong et al., 2017, 2021). However, the reduction caused by low-degree of melting in the peridotite is not enough to account for U1431 samples with $\delta^{26}Mg$ values < -0.3‰, the La/Yb ratios of U1431 basalts (referring to the degree of partial melting) in Fig. 7b also show insignificant with $\delta^{26}Mg$ values. Therefore, the degree of partial melting (or partial melting) has negligible effect on the Mg isotopes of SCS MORBs. Additionally, the mantle source of U1433 basalts was suggested to have been contaminated by low continental crust (Wu et al., 2023; Zhang et al., 2018a), which may result in the enrichment of LREE. Therefore, the melting degree will be underestimated by using the elemental ratios like above and cannot be directly used. We will discuss the origin of Mg isotopes of this site basalts in the following section.

5.2.1. Origin of the light Mg isotopic compositions of U1431 basalts

Previous studies found that the ilmenites have low $\delta^{26}Mg$ values ($< -0.61 \pm 0.03$‰) and the accumulation of ilmenite in the mantle source may result in light Mg isotopic compositions of basalts (Huang et al., 2015; Sedaghatpour et al., 2013; Tian et al., 2016). Since some of the MORBs in Site U1431 have lower $\delta^{26}Mg$ values than the normal mantle, the possibility of isotopically light ilmenite accumulation in the mantle source should be considered. However, the $\delta^{26}Mg$ values of our samples in all three sites present no correlations with TiO_2 contents (Fig. 7c). The Nb and Ta are compatible elements in ilmenite and they have a partition coefficient D_{Ta}/D_{Nb} of about 1.3 between ilmenite and mafic melts (Dygert et al., 2013), thus, the Nb/Ta ratios and TiO_2 contents will show negative correlation due to the accumulation of ilmenite in the mantle source, however the opposite trend is observed (Fig. 7d). Therefore, the light Mg isotopic compositions of the U1431 basalts are unlikely to come from the ilmenite accumulation in the mantle source.

Sedimentary carbonates can be transported into the mantle by subducted slabs, and recycled carbonates in the mantle source will cause light Mg isotopes in basalts (Huang et al., 2015; Li et al., 2017; Yang et al., 2012). Marine carbonates have distinctive lower $\delta^{26}Mg$ values (-5.57‰ to -0.38‰, Teng, 2017) than the mantle (-0.25 ± 0.04‰, Teng et al., 2010), and, thus, basalts generated by mantle source involving recycled carbonates can show extremely light $\delta^{26}Mg$ from -0.66‰ to -0.48‰ (Li et al., 2021). However, most of the U1431 basalts have mantle-like $\delta^{26}Mg$ values, as we discuss later, the slightly

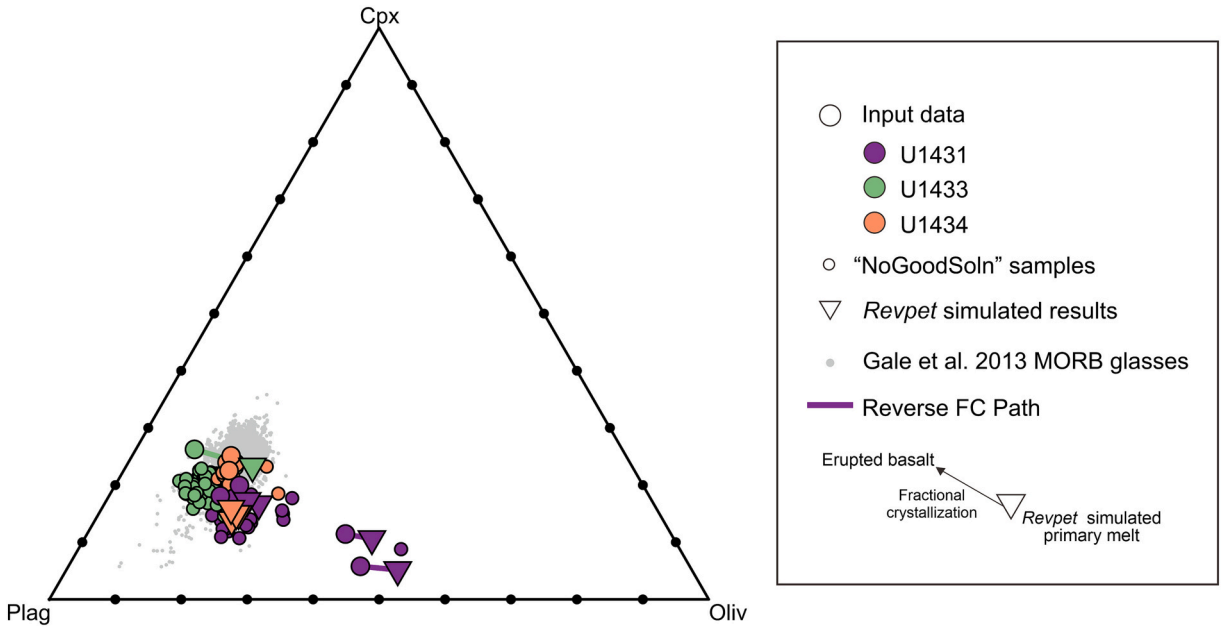

Fig. 6. The inversion fractional crystallization processes of the SCS basalts by the *Revpet*. Circles in different colour are from published data (Chen et al., 2022; Liao, 2020; Zhang et al., 2018a). Those grey points are mid-ocean ridge basalts from Gale et al. (2013). The simulated primary melts are represented by those triangles. Those straight lines indicate that they only experienced the fractional crystallization of olivine. Besides, there are many samples with a higher root mean square deviation (RMSD) error than the set value (1.5%) and expressed by little circles which were called "NoGoodSoln" in the legend. The RMSD means the error measured by the compositional distance between basalt and the *Revpet* predicted phase boundaries (Krein et al., 2021), 1.5% is the optimal threshold error of RMSD.

lower values of some high MgO samples are most likely due to their high abundance of olivine. Basalts metasomatized by carbonates have typical characteristics like high CaO/Al_2O_3 and Ba/Rb ratios, however, those of U1431 basalts are significantly lower than the reference value (Tian et al., 2016). Neither carbonate metasomatism was observed in the SCS basalts (Li et al., 2014b; Liao et al., 2022a; this study). Therefore, the contribution of recycled carbonates may be insignificant.

Carbonated peridotite can also produce melts with low δ^{26}Mg values (Li et al., 2017). The lithospheric mantle of the SCS is considered to have experienced the evolution of carbonated silicate melts to alkali basalts (Zhang et al., 2017). Experiments showed that during partial melting of carbonated peridotite, carbonated silicate melts evolve from carbonatitic melts due to increasing temperature and degree of melting (Dasgupta et al., 2007). The interaction of carbonatitic melts and silicate melts can fractionate the δ^{26}Mg features of basalts; basalts generated by low degrees of melting usually exhibit light Mg isotopic compositions as they are largely contributed by isotopically light carbonatitic melts (Huang et al., 2015). Based on previous studies, carbonated peridotite-derived melts are geochemically characterized by low Fe/Mn ratios, but high CaO/Al_2O_3 and La/Yb ratios (Huang et al., 2015; Li et al., 2017; Zeng et al., 2010), but these features are not observed in our U1431 samples with low δ^{26}Mg values. Therefore, the δ^{26}Mg variations of the SCS basalts may be neither related to carbonated peridotite.

Basaltic magmas can be generated by partial melting of either peridotite or pyroxenite. The relative proportions of pyroxenite-derived and peridotite-derived magma are mainly controlled by the degree of partial melting, because of the relatively lower melting point of pyroxenite compared to the peridotite. Generally, a lower degree of partial melting gives rise to a higher proportion of magma produced by pyroxenite. Previous study also suggested that mantle lithologies can lead to significant Mg isotopic fractionation between residue and melt (Zhong et al., 2017). The FC3MS value (FeO / CaO – 3 * MgO / SiO_2, all in wt%) has been proposed as a powerful discriminant parameter to identify most pyroxenite-derived basalts (Yang and Zhou, 2013), which is mainly affected by the source composition rather than the melting temperature and pressure. In addition, the Fe/Mn ratios in basalts can also be applied to investigate their source lithology (Liu et al., 2008). Olivine in peridotite has K_d for Fe greater than K_d for Mn, the bulk K_d changes can lower the Fe/Mn ratio of peridotite-derived melt compared with pyroxenite-derive melt (Sobolev et al., 2007). To better constrain the source lithology of our samples, we used the primary melt composition to calculate the FC3MS and Fe/Mn. As shown in Fig. 8, most of the U1431 samples plot in the peridotite field with only two of them in the pyroxenite field, indicating that U1431 basalts may be generated mainly by partial melting of a peridotite source, although a few of them may have pyroxenite in their mantle source. This is supported by the olivine geochemistry, which indicated that an eclogite−/pyroxenite-rich component may exist in the mantle source of some U1431 basalts (Zhang et al., 2018b). Furthermore, no correlation can be found between δ^{26}Mg values and elemental ratio that diagnosed of pyroxenite melts (Fig. S3d). Therefore, the light Mg isotopic compositions of U1431 basalts may not originate from the pyroxenite mantle source.

Some U1431 samples contain large amounts of olivine (Fig. 3), and we observed the phenomenon of olivine accumulation in a thin section under the microscope (349-U1431E-42R-1-W,66/68, Fig. 9). This sample (349-U1431E-42R-1-W,66/68) has particularly high MgO and Ni concentrations, which means that the olivine accumulation in the upper section basalts may occur. According to previous studies, the average δ^{26}Mg values of high-MgO (> 10 wt%) U1431 basalts are −0.29‰ to −0.28‰ (Liao et al., 2022a; Zhong et al., 2021), which are lower than the normal mantle. In olivine, the coordination number of Mg is 6 and the Mg sites are eightfold and six-coordinated (Wilding et al., 2004). Olivine has light Mg isotopic compositions due to the high Mg coordination and low Mg—O bonds (Bigeleisen and Mayer, 1947; Young et al., 2009). As shown in Fig. 4 and Fig. 9, the global basalt olivine can have a δ^{26}Mg value low as −0.336 (Hawaii green sand, Kilauea, Young et al., 2009). In Fig. 9, one of our samples with MgO > 10 wt% (349-U1431E-40R-2-W, 45.5/48) has an obviously low δ^{26}Mg value of -0.31 ± 0.01‰ and shows Ni concentration significantly higher than other samples, suggesting the high abundance of olivine. The other two samples (349-U1431E-37R-1-W,58/60 and 349-U1431E-41R-2-W,133/136) with relatively higher MgO and Ni concentrations also show lower δ^{26}Mg values than that of the normal mantle, but close to the olivine. Therefore, the low δ^{26}Mg values of our high-MgO samples are likely to reflect

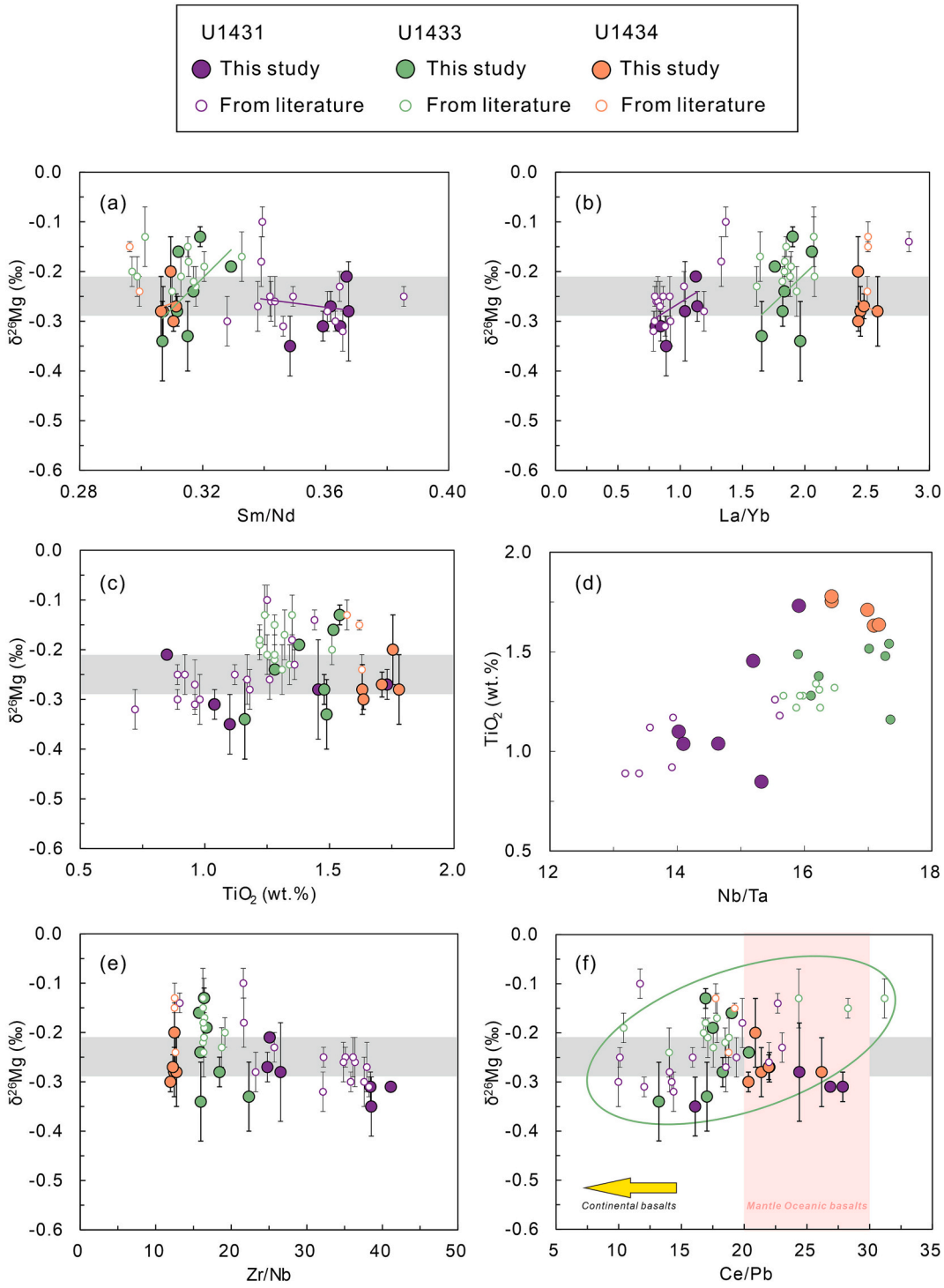

Fig. 7. (a) Sm/Nd, (b) La/Yb, (c) TiO_2, (e) Zr/Nb and (f) Ce/Pb versus $\delta^{26}Mg$ values of the studied SCS basalts. (d) Nb/Ta versus TiO_2 (wt%). Circles in larger sizes represent data in this study. Hollow circles in smaller sizes are data from other literature (Liao et al., 2022a; Zhong et al., 2021). The horizontal grey bar stands for the $\delta^{26}Mg$ values of the normal mantle (-0.25 ± 0.04‰, Teng et al., 2010), and the vertical pink bar represents the Ce/Pb values of mantle oceanic basalts (25 ± 5, Fedorov et al., 2022). The vertical black lines represent 2SD uncertainties. (For interpretation of the references to colour in this figure legend, the reader is referred to the web version of this article.)

the Mg isotopic compositions of olivine, instead of melts. This is also supported by a recent study that the Mg isotopic compositions of high-MgO basalts were affected by olivine accumulation and show similar $\delta^{26}Mg$ values to olivine separates, thus cannot represent primary magma compositions (Wang et al., 2021). On the other hand, the Mg isotopic compositions of low-MgO samples are unaffected, as they contain a small amount of olivine. Thus, in view of the light Mg isotopic composition of olivine and petrographic evidence of olivine accumulation, we attribute the slightly low $\delta^{26}Mg$ values of our U1431 basalts to the enrichment of olivine, rather than reflect their source composition.

5.2.2. *Mg isotopes of SCS basalts mirror the source heterogeneity*

The Site U1433 and U1434 are both located in the Southwest sub-basin. All of the U1433 basalts and most of the U1434 basalts plot in the

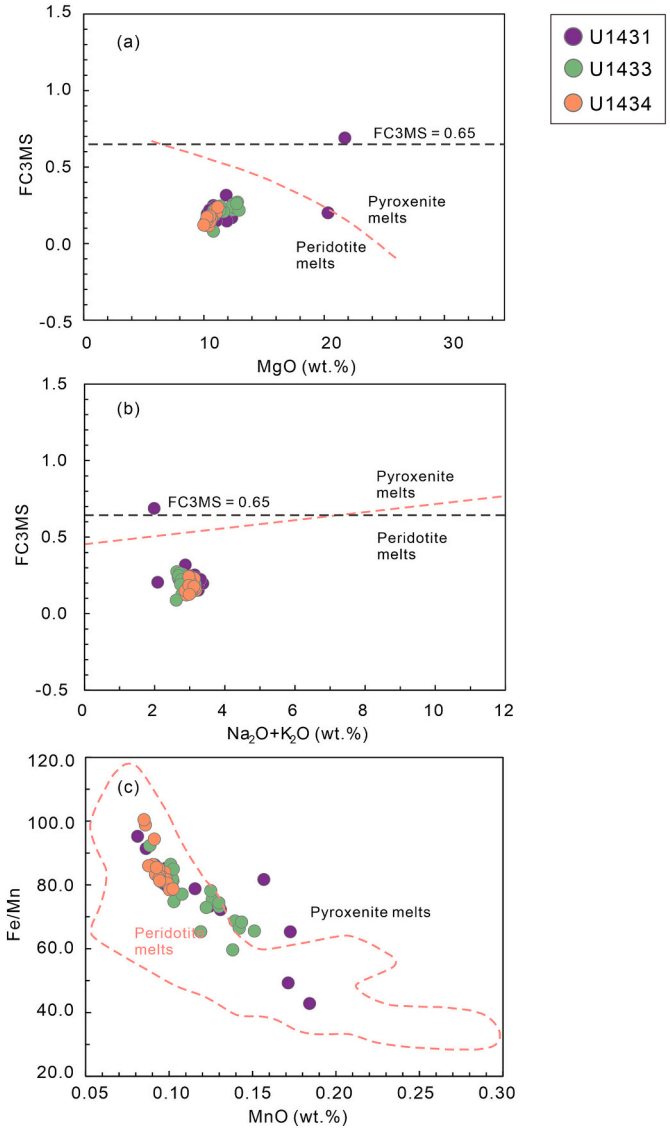

Fig. 8. (a) (b) Diagrams showing the FC3MS value as functions of MgO and $Na_2O + K_2O$. (c) Fe/Mn ratios of SCS basalts versus MnO values. The black dotted line in (a) and (b) represents a FC3MS value of 0.65, which means the upper limit for peridotite melts. The pink dotted lines in (a) and (b) are the upper boundary for peridotite melts (Yang and Zhou, 2013). Circles in different colourare from published data (Chen et al., 2022; Liao, 2020; Zhang et al., 2018a). The data used here were all calculated by the *Revpet* algorithm and represent the state of primary magma. (For interpretation of the references to colour in this figure legend, the reader is referred to the web version of this article.)

peridotite field, suggesting that the role of pyroxenite in their mantle source is insignificant (Fig. 8). The trace elemental ratios Zr/Nb and Ce/Pb have been previously used to distinguish different mantle sources (Fedorov et al., 2022). As shown in Fig. 7e and f, most of U1433 and U1434 basalts have lower Zr/Nb and Ce/Pb ratios than the U1431 basalts. Meanwhile, some of the U1433 samples have δ^{26}Mg values higher than the normal mantle, and the different Zr/Nb and Ce/Pb ratios between the U1433 and U1434 basalts may also suggest different magma sources.

Previous studies proposed that the high-δ^{26}Mg features of U1433 basalts resulted from the contribution of either sub-arc peridotitic mantle (Zhong et al., 2021) or metasomatism of subduction-released fluids (Liao et al., 2022a). The mantle source of U1433 basalts is considered to be contaminated by the lower continental crust with evidence of low Pb isotopic ratios but high εHf values (Wu et al., 2023; Zhang et al., 2018a). Previous modelling results showed that a mixing of 5% LCC with the average Pacific N-MORB can produce the isotopic composition of the U1433 basalts (Zhang et al., 2018a). The LCC shows heterogeneous Mg isotopic composition ranging widely from −0.72 to +0.19‰ (Teng et al., 2013; Yang et al., 2016). Therefore, LCC contamination may also play a role in generating the Mg isotopic compositions of U1433 basalts. Because of the similar compatibility in oceanic basalts, the Ce/Pb ratios can be used to decipher their mantle source. The Ce/Pb ratios of mantle and crustal melts are quite different, i.e., 25 ± 5 for oceanic basalts and 3–5 for continental rocks (Fedorov et al., 2022). In this study, most of the U1433 basalts have relatively lower Ce/Pb ratios than the oceanic basalts, and show a greater variation of δ^{26}Mg values (Fig. 7f), which may suggest the LCC contamination.

The δ^{26}Mg values and Ce/Pb ratios of U1434 basalts are similar to the normal mantle, suggesting that they may not be contaminated by LCC. Both of sites U1434 and U1431 are near the fossil spreading ridge. A previous study proposed that the source region of U1431 basalts may be influenced by the Hainan mantle plume (Zhang et al., 2018a). Li et al. (2017) confirmed a large-scale mantle δ^{26}Mg anomaly in eastern China, the Cenozoic basalts originating from the Hainan plume exhibit low δ^{26}Mg features. However, all the published Mg isotopic data of U1431 basalts have similar δ^{26}Mg values to the normal mantle. Previous studies proposed that such Mg isotopic composition can be generated by mixing of heavy-Mg isotopic source (sub-arc peridotitic mantle) and light-Mg isotopic source (pyroxenitic carbonated materials generated in the Hainan hotspot) (Liao et al., 2022a; Zhong et al., 2021). Therefore, we need to further constrain the role of the Hainan mantle plume in the evolution of SCS.

5.3. *The role of the Hainan mantle plume in the opening and spreading of the SCS*

As we discussed above, the Mg isotope alone is insufficient for us to fully understand the role of Hainan mantle plume in generating the SCS MORBs. The mantle plume model suggests that hot spots are driven by active thermal upwelling (Putirka et al., 2007), and the mantle potential temperature is a thermal parameter to identify the existence of a mantle plume, which refers to a hypothetic temperature that the mantle would have when magma reaches the surface through adiabatic upwelling (McKenzie and Bickle, 1988).

The Site U1500 was drilled by IODP Expedition 367/368 in the northern margin of the east subbasin of SCS, and MORB samples recovered there can reveal the condition of the mantle source during initial seafloor spreading (Yu and Liu, 2020; Zhang et al., 2021). As we discussed, nearly all the published MORBs in the SCS have experienced mineral fractional crystallization (not only olivine). So here we using the *Revpet*, which is designed for the evolved basalts (Krein et al., 2021), to calculate the melting pressure and temperature of the MORBs from Sites U1431, U1433, U1434 and U1500. We collected all the published whole-rock data of SCS MORBs for calculation (Chen et al., 2022; Liao, 2020; Liao et al., 2022b; Zhang et al., 2018a). Through determining variable potential reverse fractional crystallization paths (RFPs) and corresponding combinations of $Mg^{\#}_{OP}$ and $Mg^{\#}_{OPA}$, *Revpet* calculates the RMSD to different phase boundaries and tests whether the error exceeds the threshold value (see Fig. 6 for detailed interpretation). The algorithm will finally match a best-fit primary melt and its melting temperature (T_M), pressure (P_M), and mantle potential temperature (T_P).

Based on the major and trace element data collected from Gale et al. (2013), the melting conditions of global MORB are also calculated for comparison. The results show that there are normal MORBs with relatively constant T_P values of 1250 °C - 1350 °C, while the T_P of MORBs influenced by nearby hot spots (associated with mantle plume) can reach as high as 1600 °C. The detailed melting temperature and pressure values are listed in Supplementary Table 1. Samples from Sites U1433

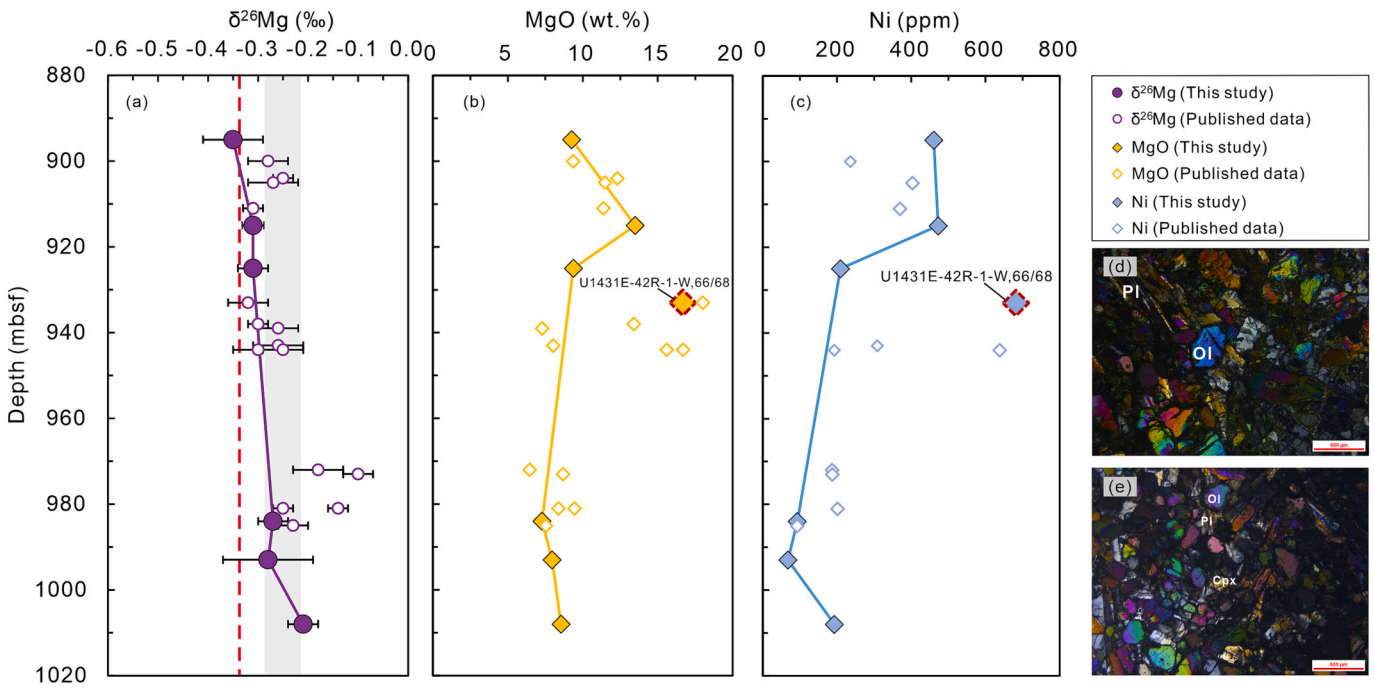

Fig. 9. (a) The δ^{26}Mg variations along with the depth of U1431 basalts; (b) The MgO variations along with the depth of U1431 basalts; (c) The Ni variations along with the depth of U1431 basalts; (d) and (e) Microscope images of the sample 349-U1431E-42R-1-W, 66/68, olivine accumulation was observed in this thin section. The rhombus in red dotted lines shows the MgO and Ni content of the sample 349-U1431E-42R-1-W, 66/68. Circles and diamonds in larger sizes represent data in this study, while those in smaller sizes and colored in white are data from other literature (Liao et al., 2022a; Zhong et al., 2021), and the red dotted line is the average δ^{26}Mg value of Hawaii basalt olivine (−0.336 ± 0.026‰, 2SE, Young et al., 2009). (For interpretation of the references to colour in this figure legend, the reader is referred to the web version of this article.)

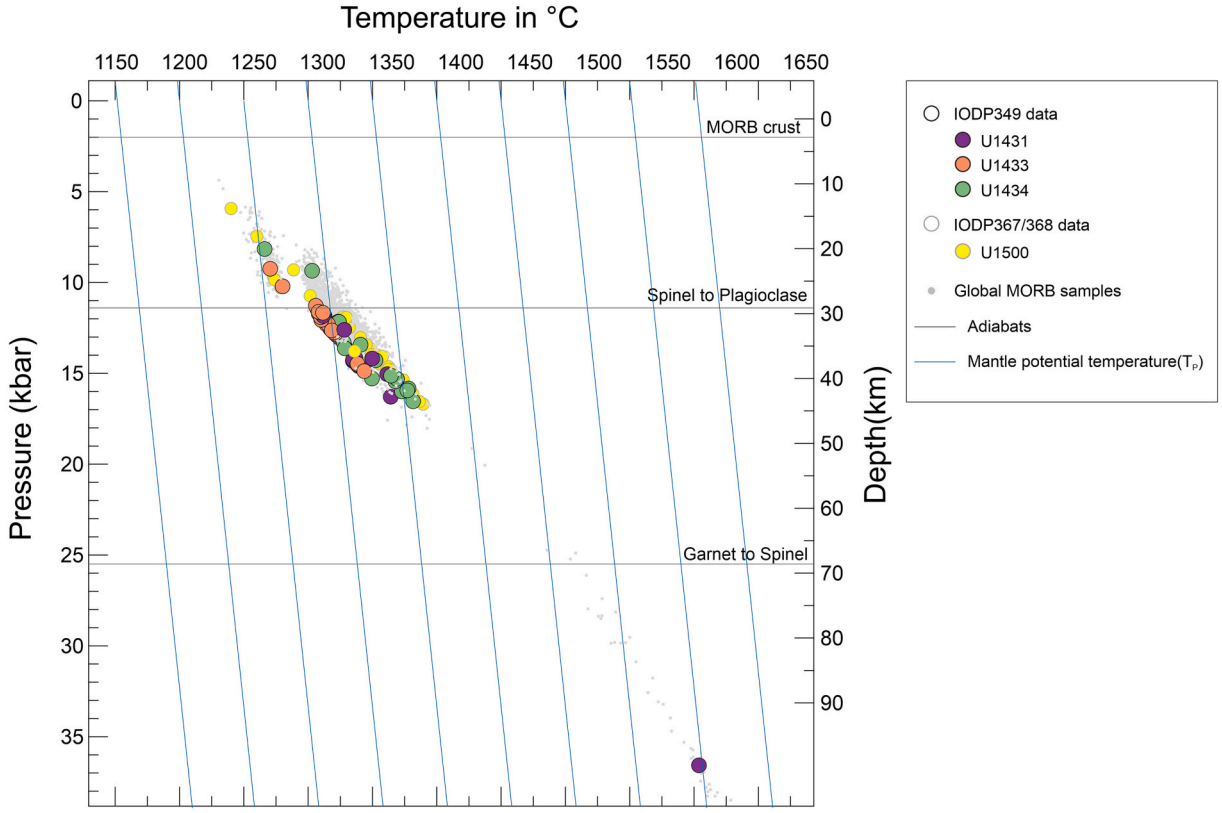

Fig. 10. The *Revpet* simulated melting temperature and pressure of SCS MORBs from different sites and global MORBs. The data of SCS MORBs in Site U1431, U1433 and U1434 are from Chen et al. (2022); Liao (2020); Zhang et al. (2018a). The data of MORBs in Site U1500 are cited from other published literature about IODP Expedition 367/368 (Chen et al., 2022; Liao et al., 2022b; Yu and Liu, 2020). The data of global MORBs are from Gale et al. (2013).

and U1434 have small variations of melting temperature and mantle potential temperature with the T_P values ranging from 1317 °C to 1357 °C, and 1257 °C to 1321 °C, respectively. These T_P values suggest that they are unlikely to be affected by mantle plume. The T_P values of basalts samples from Site U1500 are from 1231 °C to 1364 °C with an average value of 1316 °C, which is approximate to the normal global MORB with an average T_P of 1321 °C. Fig. 10 shows the melting temperature and pressure of SCS MORBs from different sites and global MORBs. No high temperature value was found in Site U1500, which means that during the early spreading stage of the SCS, there was no thermal anomaly existed.

However, samples from Site U1431 have T_P values ranging from 1294 °C to 1597 °C. There are two samples with T_P values higher than 1500 °C (U1431E-43R-2 W, 6/10 from Liao (2020) and 43R-2 from Chen et al. (2022)). They belong to the upper section basalts at Site U1431, and have high MgO contents up to 16.7 wt% and 17.2 wt%, indicating olivine accumulation. Those olivine phenocrysts most likely crystallized early in the magma chamber and their compositions were not in equilibrium with the bulk-rock, which is consistent with the petrogenesis of the U1431 upper section basalts with high MgO contents (Zhang et al., 2018b). This notion is also highly consistent with the low δ^{26}Mg values of such high MgO Site U1431 basalts. In summary, the *Revpet* predicts mantle melting conditions from olivine melt composition (Krein et al., 2021), but it depends on the input whole-rock data. The disequilibrium of whole-rock and olivine composition may cause an overestimation of the T_P. In the Site U1431 case, the high-T signatures of the two high-MgO basalts are meaningless. Therefore, the whole-rock major elements do not support the scenario that the mantle plume affected the source of U1431 MORBs.

Overall, all the published whole-rock major elements may not support the role of mantle plume in the evolution history of SCS.

6. Conclusion

The Mg isotopic compositions of the SCS basalts show heterogeneity on three sites. The δ^{26}Mg values of some Site U1431 basalts are slightly lower than that of the normal mantle, and this may due to the enrichment of olivine. The basalts in Site U1433 have been contaminated by the lower continental crust on the basis of trace elemental ratios and most variable δ^{26}Mg values. According to the *Revpet* calculation, the SCS basalts have normal mantle potential temperatures. Therefore, the role of mantle plume in the opening and spreading of the SCS may be insignificant.

Supplementary data to this article can be found online at https://doi.org/10.1016/j.margeo.2023.107164.

Declaration of Competing Interest

We have no known competing financial interests or personal relationships that could have appeared to influence the work reported in this paper.

Data availability

All data in this study are included in the article and supplementary material, they are also available in the Mendeley database (doi: 10.17632/ppfpg3yn25.1).

Acknowledgements

We gratefully thank four anonymous reviewers for their thorough and constructive comments, and Editor-in-Chief Adina Paytan for the editorial handling, which greatly improve the quality of this manuscript. This study was supported by the National Natural Science Foundation of China (Nos. 42072069) and the Natural Science Foundation of Hainan Province, China (nos.521QN274 and 421CXTD441).

References

An, Y., Fei, W., Xiang, Y., Nan, X., Fang, H., 2014. High-precision Mg isotope analyses of low-Mg rocks by MC-ICP-MS. Chem. Geol. 390, 9–21. https://doi.org/10.1016/j.chemgeo.2014.09.014.

Berglund, M., Wieser, M.E., 2011. Isotopic compositions of the elements 2009 (IUPAC Technical Report). Pure Appl. Chem. 83 (2), 397–410. https://doi.org/10.1351/pac-rep-10-06-02.

Bigeleisen, J., Mayer, M.G., 1947. Calculation of equilibrium constants for isotopic exchange reactions. J. Chem. Phys. 15 (5), 261–267. https://doi.org/10.1063/1.1746492.

Chen, S.-S., Chen, J., Guo, Z., Wu, T., Liu, J., Gao, R., 2022. Magma evolution of the South China Sea basin from continental-margin rifting to oceanic crustal spreading: Constraints from In-situ trace elements and Sr isotope of minerals. Chem. Geol. 589, 120680 https://doi.org/10.1016/j.chemgeo.2021.120680.

Cullen, A., Reemst, P., Henstra, G., Gozzard, S., Ray, A., 2010. Rifting of the South China Sea: new perspectives. Pet. Geosci. 16 (3), 273–282. https://doi.org/10.1144/1354-079309-908.

Dasgupta, R., Hirschmann, M.M., Smith, N.D., 2007. Partial Melting experiments of Peridotite + CO_2 at 3 GPa and Genesis of Alkalic Ocean Island Basalts. J. Petrol. 48 (11), 2093–2124. https://doi.org/10.1093/petrology/egm053.

Ding, W., Li, J., Clift, P.D., 2016. Spreading dynamics and sedimentary process of the Southwest Sub-basin, South China Sea: Constraints from multi-channel seismic data and IODP Expedition 349. J. Asian Earth Sci. 115, 97–113. https://doi.org/10.1016/j.jseaes.2015.09.013.

Ding, W., Sun, Z., Dadd, K., Fang, Y., Li, J., 2018. Structures within the oceanic crust of the central South China Sea basin and their implications for oceanic accretionary processes. Earth Planet. Sci. Lett. 488, 115–125. https://doi.org/10.1016/j.epsl.2018.02.011.

Dygert, N., Liang, Y., Hess, P., 2013. The importance of melt TiO_2 in affecting major and trace element partitioning between Fe-Ti oxides and lunar picritic glass melts. Geochim. Cosmochim. Acta 106, 134–151. https://doi.org/10.1016/j.gca.2012.12.005.

Fedorov, P.I., Koloskov, A.V., Beliatsky, B.V., Golovneva, L.B., 2022. A spatiotemporal change in deep sources for cenozoic volcanic rocks in the Eastern Koryak Highlands. Russ. J. Pac. Geol. 16 (3), 173–187. https://doi.org/10.1134/S1819714022030034.

Flower, M.F.J., Tamaki, K., Hoang, N., 1998. Mantle extrusion: a model for dispersed volcanism and DUPAL-like asthenosphere in East Asia and the western Pacific. In: Mantle Dynamics and Plate Interactions in East Asia, pp. 67–88. https://doi.org/10.1029/gd027p0067.

Foster, G.L., Pogge von Strandmann, P.A.E., Rae, J.W.B., 2010. Boron and magnesium isotopic composition of seawater. Geochem. Geophys. Geosyst. 11 (8) https://doi.org/10.1029/2010gc003201.

Franke, D., Savva, D., Pubellier, M., Steuer, S., Mouly, B., Auxietre, J.-L., Meresse, F., Chamot-Rooke, N., 2014. The final rifting evolution in the South China Sea. Mar. Pet. Geol. 58, 704–720. https://doi.org/10.1016/j.marpetgeo.2013.11.020.

Gale, A., Dalton, C.A., Langmuir, C.H., Su, Y., Schilling, J.-G., 2013. The mean composition of ocean ridge basalts. Geochem. Geophys. Geosyst. 14 (3), 489–518. https://doi.org/10.1029/2012GC004334.

Guo, B., Zhu, X., Dong, A., Yan, B., Shi, G., Zhao, Z., 2019. Mg isotopic systematics and geochemical applications: a critical review. J. Asian Earth Sci. 176, 368–385. https://doi.org/10.1016/j.jseaes.2019.03.001.

Higgins, J.A., Schrag, D.P., 2010. Constraining magnesium cycling in marine sediments using magnesium isotopes. Geochim. Cosmochim. Acta 74, 5039–5053. https://doi.org/10.1016/j.gca.2010.05.019.

Hofmann, A.W., 1997. Mantle geochemistry: the message from oceanic volcanism. Nature 385 (6613), 219–229. https://doi.org/10.1038/385219a0.

Hofmann, A.W., Jochum, K.P., Seufert, M., White, W.M., 1986. Nb and Pb in oceanic basalts: new constraints on mantle evolution. Earth Planet. Sci. Lett. 79 (1–2), 33–45. https://doi.org/10.1016/0012-821x(86)90038-5.

Huang, J., Li, S.-G., Xiao, Y., Ke, S., Li, W.-Y., Tian, Y., 2015. Origin of low δ^{26}Mg Cenozoic basalts from South China Block and their geodynamic implications. Geochim. Cosmochim. Acta 164, 298–317. https://doi.org/10.1016/j.gca.2015.04.054.

Huang, C., Gu, H.-O., Sun, H., Wang, F., Chen, B., 2021. High-precision determination of stable potassium and magnesium isotopes utilizing single column separation and multicollector inductively coupled plasma mass spectrometry. Spectrochim. Acta B At. Spectrosc. 181, 106232 https://doi.org/10.1016/j.sab.2021.106232.

Jochum, K.P., Verma, S.P., 1996. Extreme enrichment of Sb, Tl and other trace elements in altered MORB. Chem. Geol. 130 (3–4), 289–299. https://doi.org/10.1016/0009-2541(96)00014-9.

Krein, S.B., Molitor, Z., Grove, T.L., 2021. *ReversePetrogen*: a multiphase dry reverse fractional crystallization-mantle melting thermobarometer applied to 13,589 mid-ocean ridge basalt glasses. J. Geophys. Res.-Solid Earth. 126 (8) https://doi.org/10.1029/2020jb021292.

Langmuir, C.H., Hanson, G.N., 1980. An evaluation of major element heterogeneity in the mantle sources of basalts. Philos. Trans. R. Soc. London Ser. A 297, 383–407. https://doi.org/10.1098/rsta.1980.0223.

le Roux, P.J., le Roex, A.P., Schilling, J.-G., Shimizu, N., Perkins, W.W., Pearce, N.J.G., 2002. Mantle heterogeneity beneath the southern Mid-Atlantic Ridge: trace element evidence for contamination of ambient asthenospheric mantle. Earth Planet. Sci. Lett. 203 (1), 479–498. https://doi.org/10.1016/s0012-821x(02)00832-4.

Li, N., Yan, Q., Chen, Z., Shi, X., 2013. Geochemistry and petrogenesis of Quaternary volcanism from the islets in the eastern Beibu Gulf: evidence for Hainan plume. Acta Oceanol. Sin. 32 (12), 40–49. https://doi.org/10.1007/s13131-013-0386-1.

Li, C.-F., Xu, X., Lin, J., Sun, Z., Zhu, J., Yao, Y., Zhao, X., Liu, Q., Kulhanek, D.K., Wang, J., Song, T., Zhao, J., Qiu, N., Guan, Y., Zhou, Z., Williams, T., Bao, R., Briais, A., Brown, E.A., Chen, Y., Clift, P., Colwell, F., Dadd, K., Ding, W., Almeida, I., Huang, X., Hyun, S., Jiang, T., Koppers, A., Li, Q., Liu, C., Liu, Z., Nagai, R., PeleoAlampay, A., Su, X., Tejada, M., Trinh, H., Yeh, Y., Zhang, C., Zhang, F., Zhang, G., 2014a. Ages and magnetic structures of the South China Sea constrained by deep tow magnetic surveys and IODP Expedition 349. Geochem. Geophys. Geosyst. 15 (12), 4958–4983. https://doi.org/10.1002/2014GC005567.

Li, C.-F., Lin, J., Kulhanek, D.K., 2014b. South China Sea tectonics: opening of the South China Sea and its implications for southeast Asian tectonics, climates, and deep mantle processes since the late Mesozoic. Int. Ocean Drilling Program Prelim. Rep. 349, 1–109. https://doi.org/10.14379/iodp.pr.349.2014.

Li, S.-G., Yang, W., Ke, S., Meng, X., Tian, H., Xu, L., He, Y., Huang, J., Wang, X.-C., Xia, Q., Sun, W., Yang, X., Ren, Z.-Y., Wei, H., Liu, Y., Meng, F., Yan, J., 2017. Deep carbon cycles constrained by a large-scale mantle Mg isotope anomaly in eastern China. Natl. Sci. Rev. 4 (1), 111–120. https://doi.org/10.1093/nsr/nww070.

Li, M.-L., Liu, S.-A., Lee, H.-Y., Yang, C., Wang, Z.-Z., 2021. Magnesium and zinc isotopic anomaly of Cenozoic lavas in Central Myanmar: Origins and implications for deep carbon recycling. Lithos 386-387, 106011. https://doi.org/10.1016/j.lithos.2021.106011.

Liao, R., 2020. Geochemical Characteristics of Cenozoic Basalts from the South China Sea and Implications for Magma Evolution. Ph. D. Thesis. Institute of Oceanology, Chinese Academy of Sciences (In Chinese with English Abstract).

Liao, R., Zhu, H., Zhang, L., Li, H., Li, C., He, Y., Sun, W., Liu, H., 2022a. Unusual δ^{26}Mg values in oceanic crust basalts from the South China Sea. GSA Bull. 135, 523–533. https://doi.org/10.1130/B36320.1.

Liao, R., Zhu, H., Li, C., Sun, W., 2022b. Geochemistry of mantle source during the initial expansion and its implications for the opening of the South China Sea. Mar. Geol. 447, 106798 https://doi.org/10.1016/j.margeo.2022.106798.

Liu, Y., Gao, S., Kelemen, P.B., Xu, W., 2008. Recycled crust controls contrasting source compositions of Mesozoic and Cenozoic basalts in the North China Craton. Geochim. Cosmochim. Acta 72 (9), 2349–2376. https://doi.org/10.1016/j.gca.2008.02.018.

McDonough, W.F., Sun, S.S., 1995. The composition of the Earth. Chem. Geol. 120 (3–4), 223–253. https://doi.org/10.1016/0009-2541(94)00140-4.

McKenzie, D., Bickle, M.J., 1988. The volume and Composition of Melt Generated by Extension of the Lithosphere. J. Petrol. 29 (3), 625–679. https://doi.org/10.1093/petrology/29.3.625.

Millero, F.J., 1974. The physical chemistry of seawater. Annu. Rev. Earth Planet. Sci. 2, 101–150. https://doi.org/10.1146/annurev.ea.02.050174.000533.

Natland, J.H., 1989. Partial melting of a lithologically heterogeneous mantle: inferences from crystallization histories of magnesian abyssal tholeiites from the Siqueiros Fracture Zone. Geol. Soc. Lond. Spec. Publ. 42, 41–70. https://doi.org/10.1144/GSL.SP.1989.042.01.05.

Niu, Y., 2016. The meaning of global ocean ridge basalt major element compositions. J. Petrol. 57 (11−12), 2081–2103. https://doi.org/10.1093/petrology/egw073.

Niu, Y., Waggoner, D.G., Sinton, J.M., Mahoney, J.J., 1996. Mantle source heterogeneity and melting processes beneath seafloor spreading centers: the East Pacific rise, 18°-19°S. J. Geophys. Res.-Solid Earth. 101 (B12), 27711–27733. https://doi.org/10.1029/96jb01923.

Putirka, K.D., Perfit, M., Jackson, M.G., 2007. Ambient and excess mantle temperatures, olivine thermometry, and active vs. passive upwelling. Chem. Geol. 241 (3–4), 177–206. https://doi.org/10.1016/j.chemgeo.2007.01.014.

Qian, S., Zhou, H., Zhang, L., Cheng, R., 2020. Mantle heterogeneity beneath the South China Sea: Chemical and isotopic evidence for contamination of ambient asthenospheric mantle. Lithos 354-355, 105335. https://doi.org/10.1016/j.lithos.2019.105335.

Rubin, K.H., Sinton, J.M., 2007. Inferences on mid-ocean ridge thermal and magmatic structure from MORB compositions. Earth Planet. Sci. Lett. 260 (1–2), 257–276. https://doi.org/10.1016/j.epsl.2007.05.035.

Rudnick, R.L., Fountain, D.M., 1985. 1995. Nature and composition of the continental crust; a lower crustal perspective. Rev. Geophys. 33 (3), 267–309. https://doi.org/10.1029/95RG01302.

Sedaghatpour, F., Teng, F.-Z., Liu, Y., Derek, Taylor, 2013. Magnesium isotopic composition of the Moon. Geochim. Cosmochim. Acta 120, 1–16. https://doi.org/10.1016/j.gca.2013.06.026.

Sobolev, A.V., Hofmann, A.W., Kuzmin, D.V., Yaxley, G.M., Arndt, N.T., Chung, S.-L., Danyushevsky, L.V., Elliott, T., Frey, F.A., Garcia, M.O., Gurenko, A.A., Kamenetsky, V.S., Kerr, A.C., Krivolutskaya, N.A., Matvienkov, V.V., Nikogosian, I. K., Rocholl, A., Sigurdsson, I.A., Sushchevskaya, N.M., Teklay, M., 2007. The amount of recycled crust in sources of mantle-derived melts. Science 316, 412–417. https://doi.org/10.1126/science.1138113.

Sun, K., 2020. Petrogenetic and Geochemical Characteristics of the SCS MORBs and Implications for the Magmatic Processes in the Latest SCS Seafloor Spreading. Master Thesis. Zhejiang University (In Chinese with English Abstract).

Sun, S.-S., McDonough, W.F., 1989. Chemical and isotopic systematics of oceanic basalts: implications for mantle composition and processes. Geol. Soc. Lond. Spec. Publ. 42 (1), 313–345. https://doi.org/10.1144/gsl.sp.1989.042.01.19.

Sun, K., Wu, T., Liu, X., Chen, X.-G., Li, C.-F., 2020. Lithogeochemistry of the mid-ocean ridge basalts near the fossil ridge of the southwest sub-basin, South China Sea. Minerals 10 (5), 465. https://doi.org/10.3390/min10050465.

Teng, F.-Z., 2017. Magnesium isotope geochemistry. Rev. Mineral. Geochem. 82 (1), 219–287. https://doi.org/10.2138/rmg.2017.82.7.

Teng, F.-Z., Wadhwa, M., Helz, R.T., 2007. Investigation of magnesium isotope fractionation during basalt differentiation: Implications for a chondritic composition of the terrestrial mantle. Earth Planet. Sci. Lett. 261 (1–2), 84–92. https://doi.org/10.1016/j.epsl.2007.06.004.

Teng, F.-Z., Li, W.-Y., Ke, S., Marty, B., Dauphas, N., Huang, S., Wu, F.-Y., Pourmand, A., 2010. Magnesium isotopic composition of the Earth and chondrites. Geochim. Cosmochim. Acta 74 (14), 4150–4166. https://doi.org/10.1016/j.gca.2010.04.019.

Teng, F.-Z., Yang, W., Rudnick, R.L., Hu, Y., 2013. Heterogeneous magnesium isotopic composition of the lower continental crust: a xenolith perspective. Geochem. Geophys. Geosyst. 14 (9), 3844–3856. https://doi.org/10.1002/ggge.20238.

Tian, H.-C., Yang, W., Li, S.-G., Ke, S., Chu, Z.-Y., 2016. Origin of low δ^{26}Mg basalts with EM-I component: evidence for interaction between enriched lithosphere and carbonated asthenosphere. Geochim. Cosmochim. Acta 188, 93–105. https://doi.org/10.1016/j.gca.2016.05.021.

Verma, S.P., 1981. Seawater alteration effects on ^{87}Sr/^{86}S, K, Rb, Cs, Ba and Sr in oceanic igneous rocks. Chem. Geol. 34 (1–2), 81–89. https://doi.org/10.1016/0009-2541(81)90073-5.

Verma, S.P., 1992. Seawater alteration effects on REE, K, Rb, Cs, Sr, U, Th, Pb and Sr-Nd-Pb isotope systematics of Mid-Ocean Ridge Basalt. Geochem. J. 26 (3), 159–177. https://doi.org/10.2343/geochemj.26.159.

Wang, X.-J., Chen, L.-H., Hanyu, T., Zhong, Y., Shi, J.-H., Liu, X.-W., Kawabata, H., Zeng, G., Xie, L.-W., 2021. Magnesium isotopic fractionation during basalt differentiation as recorded by evolved magmas. Earth Planet. Sci. Lett. 565, 116954 https://doi.org/10.1016/j.epsl.2021.116954.

Wilding, M.C., Benmore, C.J., Tangeman, J.A., Sampath, S., 2004. Evidence of different structures in magnesium silicate liquids: coordination changes in forsterite- to enstatite-composition glasses. Chem. Geol. 213 (1), 281–291. https://doi.org/10.1016/j.chemgeo.2004.08.055.

Wu, T., Zhang, W., Wilde, S.A., Lu, J., Zhang, G., Li, C., Chen, X., Chen, S., 2023. Highly unradiogenic Pb isotopes revealed by plagioclase-hosted melt inclusions in E-MORB from the South China Sea. J. Geophys. Res.-Solid Earth. 128 (4) https://doi.org/10.1029/2022JB025348.

Xu, Y., Wei, J., Qiu, H., Zhang, H., Huang, X., 2012. Opening and evolution of the South China Sea constrained by studies on volcanic rocks: preliminary results and a research design. Chin. Sci. Bull. 57 (24), 3150–3164. https://doi.org/10.1007/s11434-011-4921-1.

Yan, P., Deng, H., Liu, H., Zhang, Z., Jiang, Y., 2006. The temporal and spatial distribution of volcanism in the South China Sea region. J. Asian Earth Sci. 27 (5), 647–659. https://doi.org/10.1016/j.jseaes.2005.06.005.

Yang, Z.-F., Zhou, J.-H., 2013. Can we identify source lithology of basalt? Sci. Rep. 3 (1) https://doi.org/10.1038/srep01856.

Yang, W., Teng, F.-Z., Zhang, H.-F., Li, S.-G., 2012. Magnesium isotopic systematics of continental basalts from the North China craton: Implications for tracing subducted carbonate in the mantle. Chem. Geol. 328, 185–194. https://doi.org/10.1016/j.chemgeo.2012.05.018.

Yang, W., Teng, F., Li, W., Liu, S., Ke, S., Liu, Y., Zhang, H., Gao, S., 2016. Magnesium isotopic composition of the deep continental crust. Am. Mineral. 101 (2), 243–252. https://doi.org/10.2138/am-2016-5275.

Yang, F., Huang, X.-L., Xu, Y.-G., He, P.-L., 2019. Plume-ridge interaction in the South China Sea: Thermometric evidence from Hole U1431E of IODP Expedition 349. Lithos 324-325, 466–478. https://doi.org/10.1016/j.lithos.2018.11.031.

Young, E.D., Tonui, E., Manning, C.E., Schauble, E.A., Macris, C.A., 2009. Spinel-olivine magnesium isotope thermometry in the mantle and implications for the Mg isotopic composition of Earth. Earth Planet. Sci. Lett. 288 (3–4), 524–533. https://doi.org/10.1016/j.epsl.2009.10.014.

Yu, X., Liu, Z., 2020. Non-mantle-plume process caused the initial spreading of the South China Sea. Sci. Rep. 10 (1) https://doi.org/10.1038/s41598-020-65174-y.

Zeng, G., Chen, L.-H., Xu, X.-S., Jiang, S.-Y., Hofmann, A.W., 2010. Carbonated mantle sources for Cenozoic intra-plate alkaline basalts in Shandong, North China. Chem. Geol. 273 (1–2), 35–45. https://doi.org/10.1016/j.chemgeo.2010.02.009.

Zhang, G.-L., Smith-Duque, C., 2014. Seafloor basalt alteration and chemical change in the ultra thinly sedimented South Pacific. Geochem. Geophys. Geosyst. 15 (7), 3066–3080. https://doi.org/10.1002/2013gc005141.

Zhang, G.-L., Chen, L.-H., Jackson, M.G., Hofmann, A.W., 2017. Evolution of carbonated melt to alkali basalt in the South China Sea. Nat. Geosci. 10 (3), 229–235. https://doi.org/10.1038/ngeo2877.

Zhang, G.-L., Luo, Q., Zhao, J., Jackson, M.G., Guo, L.-S., Zhong, L.-F., 2018a. Geochemical nature of sub-ridge mantle and opening dynamics of the South China Sea. Earth Planet. Sci. Lett. 489, 145–155. https://doi.org/10.1016/j.epsl.2018.02.040.

Zhang, G.-L., Sun, W.-D., Seward, G., 2018b. Mantle source and magmatic evolution of the dying spreading ridge in the South China Sea. Geochem. Geophys. Geosyst. 19 (11), 4385–4399. https://doi.org/10.1029/2018GC007570.

Zhang, Y., Yu, K., Fan, T., Yue, Y., Wang, R., Jiang, W., Xu, S., Wang, Y., 2020. Geochemistry and petrogenesis of Quaternary basalts from Weizhou Island, northwestern South China Sea: evidence for the Hainan plume. Lithos 362-363, 105493. https://doi.org/10.1016/j.lithos.2020.105493.

Zhang, X., Lin, J., Behn, M.D., 2021. Mantle heterogeneity and melting processes in the South China Sea: thermal and melting models constrained by oceanic crustal thickness and basalt geochemistry. J. Geophys. Res.-Solid Earth. 126 (2) https://doi.org/10.1029/2020JB020735.

Zhong, Y., Chen, L.-H., Wang, X.-J., Zhang, G.-L., Xie, L.-W., Zeng, G., 2017. Magnesium isotopic variation of oceanic island basalts generated by partial melting and crustal recycling. Earth Planet. Sci. Lett. 463, 127–135. https://doi.org/10.1016/j.epsl.2017.01.040.

Zhong, Y., Zhang, G.-L., Jin, Q.-Z., Huang, F., Wang, X.-J., Xie, L.-W., 2021. Sub-basin scale inhomogeneity of mantle in the South China Sea revealed by magnesium isotopes. Sci. Bull. 66, 740–748. https://doi.org/10.1016/j.scib.2020.12.016.